Lab on a Chip

Cite this: *Lab Chip*, 2012, **12**, 5243–5248

www.rsc.org/loc

PAPER

A microfluidic-based bubble generation platform enables analysis of physical property change in phospholipid surfactant layers by interfacial ozone reaction†

Young Shik Shin,[abc] Tae Su Choi,[d] Hyungjun Kim,[e] J. L. Beauchamp,[b] James R. Heath[abc] and Hugh I. Kim*[d]

Received 17th August 2012, Accepted 16th October 2012
DOI: 10.1039/c2lc40940b

The air-liquid interface filled with pulmonary surfactant is a unique feature of our lung alveoli. The mechanical properties of this interface play an important role in breathing and its malfunction induced by an environmental hazard, such as ozone, relates to various lung diseases. In order to understand the interfacial physics of the pulmonary surfactant system, we employed a microfluidic bubble generation platform with a model pulmonary surfactant composed of two major phospholipids: DPPC (1,2-dipalmitoyl-*sn*-phosphatidylcholine) and POPG (1-palmitoyl-2-oleoyl-*sn*-phosphatidylglycerol). With fluorescence imaging, we observed the ozone-induced chemical modification of the unsaturated lipid component of the lipid mixture, POPG. This chemical change due to the oxidative stress was further utilized to study the physical characteristics of the interface through the bubble formation process. The physical property change was evaluated through the oscillatory behaviour of the monolayer, as well as the bubble size and formation time. The results presented demonstrate the potential of this platform to study interfacial physics of lung surfactant system under various environmental challenges, both qualitatively and quantitatively.

Introduction

In recent years, microfluidics has been demonstrated as a powerful and practical tool for generating microdroplets and microbubbles.[1–3] Due to their small size, highly reproducible formation process and controllability, microdroplets are utilized in various applications, including the encapsulation and reaction of bio-components, such as proteins,[4–6] DNAs[2] and cells.[7,8] Microbubbles, however, have been utilized mainly as medical imaging contrast agents and studies have focused more on how to generate microbubbles in a controllable and high throughput manner.[9,10] Studying the interfacial physics through the bubble generation process has recently been the major study topic rather than applications.[11–14] Here, however, we focus on the characteristic of the air–liquid interface in a new application using the formation process of microbubbles, as well as their physical properties.

The air–liquid interface is an interesting topic in fundamental physics, but it also plays an important role in biology. One of the major examples is the cardiopulmonary system. The cardiopulmonary system is constantly exposed to airborne environmental hazards. The short- and long-term exposure of lungs to irritants, such as pathogens and air pollutants, can cause acute and chronic injuries.[15–17] Such exposures occur at the air–liquid interface of the pulmonary surfactant (PS) system, which provides the first barrier of our lungs to an environmental challenge. The PS is a mixture of lipids and proteins that participates in the breathing cycle, but also prevents lung collapse by reducing the surface tension of the alveolar sacs. Thus, the physical and chemical characteristics of the interfacial PS system are of high interest. Microbubbles are a valuable tool for this application because they can be modified to resemble a PS interface. Microbubbles can also provide a platform for the detailed investigation of interfacial dynamics.[11–14]

We demonstrate an application of microbubbles, controlled within microfluidic systems, towards understanding the physical properties of alveolar sacs, especially under oxidative stress. Ozone has been reported as a representative source of air pollution that is associated with the risk of death from respiratory illness.[15] Several groups have reported on the influence of ozone-induced oxidative stress on the chemistry of the air–liquid interfacial PS, and have found that this exhibits characteristics that are distinct from the solution phase.[18–20] The

[a]*Nanosystems Biology Cancer Center, California Institute of Technology, MC 127-72, Pasadena, California 91125, USA*
[b]*Division of Chemistry and Chemical Engineering, California Institute of Technology, MC 127-72, Pasadena, California 91125, USA*
[c]*Molecular and Medical Pharmacology, University of California, Los Angeles, California 90095, USA*
[d]*Department of Chemistry, Pohang University of Science and Technology (POSTECH), Pohang, 790-784, Republic of Korea. E-mail: hughkim@postech.edu; Fax: +82-54-279-3399; Tel: +82-054-279-2341*
[e]*Graduate School of EEWS, Korea Advanced Institute of Science and Technology, Daejeon, 305-701, Republic of Korea*
† Electronic Supplementary Information (ESI) available: Supplementary method, Fig. S1–S6, Table 1–2 and Movie 1–2. See DOI: 10.1039/c2lc40940b

above cited investigations focused on selective molecular transformations that occur as a result of oxidative stress only at the interface. Such molecular transformations can have a strong influence on the physical properties of the PS system (*e.g.* the surface tension and elasticity of the PS interface), and so understanding how chemical transformations influence such physical properties can provide key insights into how the PS system responds to environmental challenges. For this purpose, we employed a microfluidic bubble generation platform with a model PS system composed of two major phospholipids: DPPC (1,2-dipalmitoyl-*sn*-phosphatidyl choline) and POPG (1-palmitoyl-2-oleoyl-*sn*-phosphatidyl glycerol), which is exposed to the condition of normal air and air containing ~20 ppm ozone.

Experimental methods

Design and fabrication of the microfluidic device

The microfluidic device was fabricated with PDMS (polydimethylsiloxane, Silgard 184, Dow Chemical, MI, USA) by standard soft lithography.[21] SU-8 (MicroChem, MA, USA) patterned wafer was used as a mold to cast PDMS into the microchannel device. The microfluidics design was based on a flow focusing device (FFD)[22] combined with a straight channel perpendicular to the bubble formation component. The height and width of the main channel were both 200 μm, and the narrow channel for bubble generation was 60 μm. Detailed design parameters can be found in Fig. S1.† The PDMS was solvent extracted just prior to bonding in order to prolong its hydrophilicity following plasma treatment.[23] The molded PDMS and a bare glass slide were both treated with oxygen plasma and bonded together to form the completed microfluidics chip. The microchannels were filled with water immediately following the bonding step in order to further maintain hydrophilicity of the surface.[22]

Bubble formation tests and analysis

Sodium salts of DPPC (1,2-dipalmitoyl-*sn*-phosphatidylcholine), POPG (1-palmitoyl-2-oleoyl-*sn*-phosphatidylglycerol) and NBD-PG (1-oleoyl-2-[12-[(7-nitro-2-1,3-benzoxadiazol-4-yl)amino]dodecanoyl]-*sn*-glycerol-3-[phospho-*rac*-(1-glycerol)]) were purchased from Avanti Polar Lipid (Alabaster, AL). Nitrobenzoxadiazole (NBD) is a widely used fluorophore that has an excitation at 470 nm and an emission at 540 nm.[24] The lipid sample was prepared by mixing 20 μM DPPC and 20 μM POPG in 1 × PBS solution. The sample solutions with small unilamellar vesicles (SUVs) were prepared by a number of freeze-thaw cycles. The hydrated lipid solution is then extruded through 100 nm polycarbonate membrane filters at room temperature. The average size of the SUV is measured as 62(±25) nm using the dynamic light scattering method. The parameters for the bubble generation were optimized for ambient (including standard atmospheric air composition) conditions. The microfluidic device, as well as the gas and liquid introduction systems, is shown in Fig. 1. A syringe pump (Fig. 1A) was utilized to flow the lipid sample into the device at a constant flow rate of 7 μl min^{-1}. The air or air/ozone mixture was injected at a constant pressure, 0.42 psi. Ozone was generated by a pencil-style UV calibration lamp (model 6035, Oriel) that was placed upstream of the pressure regulator. By turning on the UV lamp, air flow was converted to ozone flow. Ozone concentration was measured spectrophotometrically and maintained at 20 ppm.

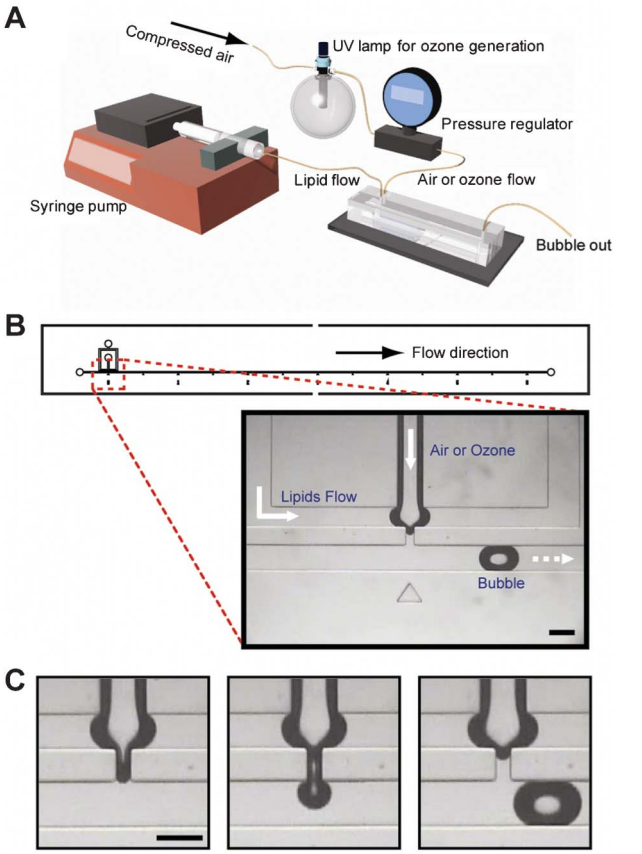

Fig. 1 (A) The experimental setup for the bubble generation and ozone effect test. (B) The microfluidic device design for the bubble generation and the zoomed-in image of the bubble formation component. Air or ozone was injected from the center channel and lipid mixture was flowed from the outer two channels. The width of the narrow thread channel is 60 μm and the main flow channel for bubbles is 200 μm. (C) Representative pictures of the bubble formation process. Bubbles are generated through a pinch-off process in a reproducible manner. The dark regions around the air–liquid interfaces are due to the contrast difference originating from the 3D curvature of the interface. All scale bars: 200 μm.

The bubble formation process was monitored by a brightfield microscope (Nikon Eclipse TE2000) throughout the experiments (Fig. 1B and 1C) and recorded as a movie at 30 frames s^{-1} by a CCD camera. All of the images were extracted from the movie by DVDVideoSoft (DVDVideoSoft.com) and analyzed by ImageJ (NIH) for the size and the generation time of bubbles. The formation time for the first thirteen bubbles was measured for the analysis. For the bubble size analysis, the length of the bubbles was measured for the first fifteen bubbles. All experiments were performed at room temperature.

Analysis and imaging of the ozone effect

To visualize the ozone effect at the interface, fluorescently tagged PG lipid (NBD-PG) was added to the lipid sample. The lipid sample composition was 20 μM DPPC, 10 μM POPG and 10 μM

NBD-PG in 1 × PBS solution. The same flow condition as for the bubble formation test was used for monitoring the fluorescence using confocal microscopy (Nikon E800) for the air, as well as the ozone conditions. Images were averaged over 10 frames for visualization. Gray-scale intensity was measured with ImageJ.

Results and discussion

The experimental setup, device design and bubble formation process are shown in Fig. 1. The bubble generation device comprises three inlet channels: a center channel supplying gas and two outer channels supplying the lipid mixture in solution. Constant inflow of the gas and lipids mixture led to the generation of highly reproducible bubbles through a pinch-off process (Fig. 1C). Bubbles were generated with a polydispersity index of ~1% (supplementary Table 1†). The polydispersity index is defined as the standard deviation of the length of the bubble divided by the mean length of the bubble in percentage. The low polydispersity index demonstrates the consistency of bubble generation in the device, allowing us to obtain statistically meaningful results. Also, these microbubbles can be a good model for more in-depth understanding of the system owing to its air–liquid interface nature and to the similar size to the alveoli (100–300 μm). Since the bubble generation process is very sensitive to physical conditions, monitoring the bubble size and frequency of the bubble generation process became the main emphasis of this paper. This will link the chemical compositional changes to the physical characteristics of the interface, giving a complete understanding of a model PS system.

Most commonly used microfluidic devices for bubble generation are based on two geometries: T junction[13,25] and flow focusing device (FFD).[14,22] Our design is mostly based on FFD, but also has a T junction-like characteristic due to the perpendicular main flow channel to the bubble formation components (Fig. S1 and S5†). In that design, we can think of three major factors that influence bubble formation: the pressure force from gas, the shear stress induced by flow and the elastic property of the lipid monolayer (Fig. S5†).[12] The gas pressure and flow rates are fixed so the observed changes in bubble formation are associated with ozone exposure, and are induced by the influence of the ozone on the physical characteristics (interfacial tension or elasticity) of the lipid monolayer.

In order to validate the potential of our system in studying the interface, we performed a test to confirm the chemical compositional change at the interface under ozone exposure through visualization. We have previously demonstrated the heterogeneous ozonolysis of a mixture of saturated and unsaturated phospholipids at the air–liquid interface using field-induced droplet ionization mass spectrometry (FIDI-MS).[20] We found that only the unsaturated phospholipids react with ozone, forming relatively hydrophilic products, such as aldehydes and carboxylic acids. Within 30 s of formation, these products dissolve into the bulk phase, leaving only saturated phospholipid on the surface of the droplet. To confirm this chemistry in our system, we used a fluorescently tagged unsaturated lipid, NBD-PG along with the model PS system, a mixture of DPPC and POPG. For microbubble experiments, a constant flow of a lipid mixture of DPPC, POPG and NBD-PG

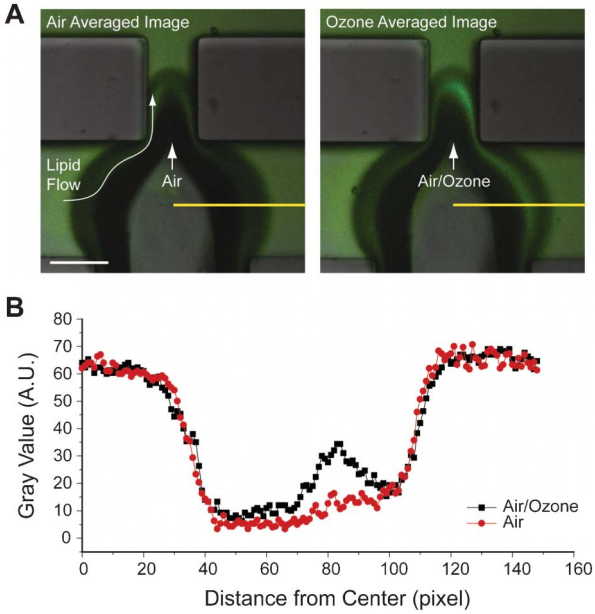

Fig. 2 The effect of ozone on the chemical composition change in the interface. (A) 10 frames averaged fluorescence images for air (left) and ozone (right) conditions. When ozone is the working gas, accumulated hydrophilic products of NBD-PG showed stronger fluorescence in the bulk phase near the interface. The dark regions around the air–liquid interfaces are due to the contrast difference originating from the 3D curvature of the interface. Scale bar: 100 μm. (B) Line profile of the gray scale intensity along the yellow lines in (A). Fluorescence intensity of the ozone condition showed about a two-fold increased value near the interface.

was maintained in the microfluidic device and either air or ozone was introduced to generate bubbles. A distinct fluorescence signal was observed in the liquid phase near the interface when ozone was introduced (Fig. 2), indicating the formation and the dissolution of hydrophilic products of NBD-PG ozonolysis into the aqueous solution around the interface. This visual detection of the chemical change of the unsaturated lipid components presents the potential of microbubbles by confirming our previous finding.[20] To make sure that the ozonolysis of NBD-PG doesn't significantly affect the result obtained in Fig. 2, we performed two ozonolysis product analyses with electrospray ionization mass spectrometry (ESI-MS): one for the mixture of DPPC, POPG and NBD-PG and the other for NBD-PG only (Fig. S2–S3†). The results show that the NBD-PG produces similar hydrophilic products to POPG in the mixture. It is notable that low abundant products from the ozonolysis of NBD-tag are also observed in the MS spectra (Fig. S2†). However, the reaction rate of ozonolysis of the probe is relatively lower than that of a C–C double bond due to its delocalization property.[26] In addition, the NBD-tag loses its intrinsic fluorescence property due to the decomposition of the conjugated ring. Hence, it is hard to expect that there is significant bias to the fluorescence image in Fig. 2 from the ozonolysis of NBD-tag (Fig. S4†). Since DPPC and POPG represent major components of saturated and unsaturated phospholipids, respectively, in our lung pulmonary surfactant system, it is interesting to see physical, as well as chemical property changes of the air–liquid interface induced by environmental stress, such as ozone. DPPC

is known as the principal phospholipid component with very low surface tension upon compression[27,28] and POPG is known to improve the adsorption and spreading of surfactant owing to their higher fluidity.[29,30] Thus, dissolving POPG into the bulk solution from the interface can change the physical characteristics of the interface, which relates to the lung physiology and disease. It is also notable that the increase in ozone concentration is associated with a higher fatality rate from respiratory illness.[15] In that sense, it is necessary to study the physical characteristics of our lung surfactant system under environmental challenges.

To achieve this goal, we move on to investigate the change of bubble formation processes, which represents physical characteristics of the interface, caused by the chemical composition alteration in a mixed lipid surfactant layer of DPPC and POPG due to the oxidative stress by ozone. The tip of the interface near the bubble formation region oscillates significantly until the bubble is ejected to the flow (Fig. 3A, 3B and supporting movie 1 and 2†). However, a significant difference was observed in a bubble formation process with ozone compared to air. Fig. 3B shows the time-lapsed trajectories of the lower tip of the interface until bubbles were formed. Stronger oscillation was observed for the case of air compared to the case of ozone. The oscillatory characteristic indicates that the elastic property of the interface is different between air and ozone conditions. To further analyze this, we can consider the effective elastic modulus (E_{eff}) defined as

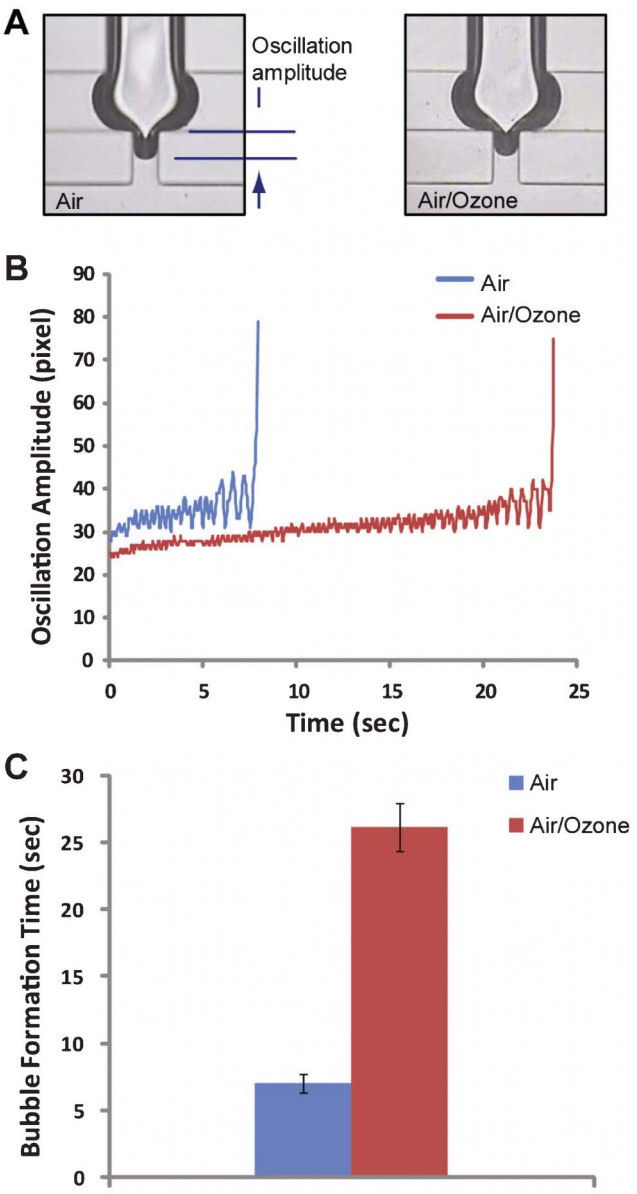

Fig. 3 (A) Snap shots of the bubble formation component after 10 frames (0.33 s) from the previous bubble formation. (B) Time-lapsed trajectories of the lower end point of the interface. Stronger oscillation for a shorter time period was observed when air was the working gas. (C) The required time for the bubble formation. The averaged time for the fifteen bubbles is shown.

$$E_{eff} = \frac{\text{stress}}{\text{strain}} \quad (1)$$

Under the assumption that the interface near the bubble formation region (in the thread) can be simplified as a cylinder (Fig. S5†), we can expect the following force balance at equilibrium based on the free body diagram (Fig. S5B†),

$$F_p + F_s = F_k \quad (2)$$

where F_p, F_s and F_k are pressure force, shear force and restoring elastic force, respectively. Using $F_p = p\pi r^2$ and $F_k = k\Delta x$, eqn (2) becomes,

$$F_s = k\Delta x - p\pi r^2 \quad (3)$$

where k is the spring constant of the monolayer, Δx is transverse displacement, p is the applied pressure and r is the radius of the cylinder. Then,

$$E_{eff} = \frac{\text{stress}}{\text{strain}} = \frac{p + F_s/2\pi rL}{\Delta x/L} \quad (4)$$

where L is the initial length of the cylinder in the thread. In the equilibrium condition, we can assume a harmonic oscillatory motion and the harmonic approximation leads to $F_k = k\Delta x = m(2\pi f)^2\Delta x$, where m is the mass of the oscillating body and f is the oscillation frequency. From eqn (3) and (4), the effective elastic modulus can be expressed as

$$E_{eff} = \frac{PL}{\Delta x}\left(1 - \frac{r}{2L}\right) + \frac{2\pi mf^2}{r} \quad (5)$$

Assuming that low concentration of ozone (~20 ppm) does not change the density of the working gas, E_{eff} becomes a function of the oscillation amplitude and the frequency. Analysis on our data in Fig. 3B shows that E_{eff} at the interface, when ozone is applied, is ~28% higher compared to the case of air. Numerical values used for the calculation can be found from the supplementary Table 2†. Thus, it appears that oxidation leads to a higher concentration of DPPC (and lower concentration of POPG) at the interfacial surfactant layer, which in turns yields a more elastic (*i.e.* resistant to deformation) interface. This increase in the elastic constant is likely primarily due to the reduced fluidity of the saturated lipids relative to the unsaturated ones, POPG. Based on an analogy with a deformation process of a material under increasing tensile stress, the bubble formation

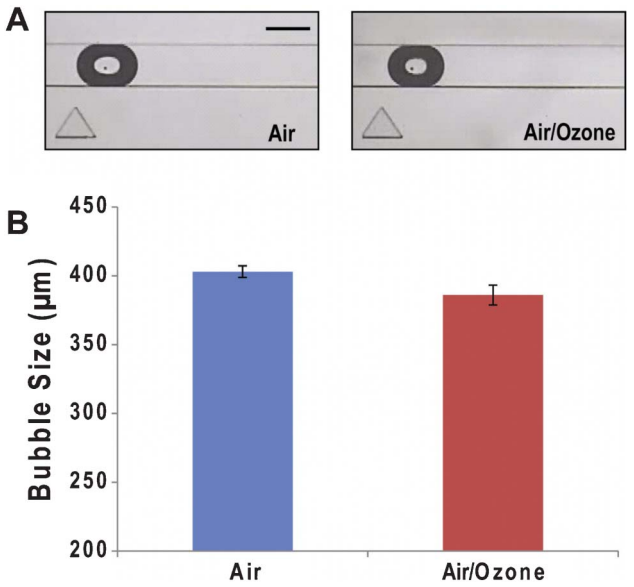

Fig. 4 Bubble size analysis. (A) Representative images of the bubbles in different conditions. Pictures were taken when bubbles flowed 20 mm downstream from the bubble formation component. Scale bar: 200 μm. (B) Bubble length in different conditions ($p < 0.0001$). The length of the bubble was measured from fifteen bubbles for the analysis.

process is similar to reaching the ultimate tensile strength (UTS). Thus, it is also interesting that we observed the increased time required for bubble formation (Fig. 3C) in the presence of ozone. This means that the ozone changes the material property of the interface, which is what we found out from the chemical analysis.

Bubble size is another metric for the physical property of the lipid surfactant layer. In Fig. 4, representative pictures of bubbles (A) and the averaged bubble sizes (B) are presented. The bubble size is smaller when ozone is the working gas. We also observed a decrease in bubble size when the mole fraction of POPG decreases to 10% of DPPC in the lipid mixture (Fig. S6†). We can think of a simple scaling of the bubble size as Garstecki *et al.* has reported previously:[12,22] $V_b \propto q_a\tau$, where V_b is the volume of the bubble, q_a is the rate of inflow gas, and τ is the time that the thread stays open until the bubble is ejected into the flow. Since τ is inversely proportional to the elasticity, we can expect that high elasticity induces shorter τ that reduces the volume of the bubble. This agrees well with our observation of increased E_{eff} and reduced size resulting from the increase of DPPC mole fraction in the surfactant layer following the heterogeneous ozonolysis of POPG. In addition to the effect of elasticity of surfactant layer, we can also examine the dynamic viscosity of the interface when the surfactant composition changes. The Hagen–Poiseuille relation, $q_a \propto p/\mu$ and $\tau \propto 1/q$ leads to $V_b \propto p/q\mu$ where μ is the dynamic viscosity and q is the volume flow rate of the solution. Since p and q are fixed in our experiment, we can compare the dynamic viscosity for both conditions simply by measuring bubble size. From the measured bubble scale, we found that the dynamic viscosity of the surfactant layer was increased by ~4.4% when ozone was used compared to pure air for bubble formation. This analysis shows that the bubble formation process is very sensitive to the alterations of the lipid compositions in the surfactant layers and has a potential for the analytical tool to study the interface physics.

Conclusions

We have developed a microfluidic bubble generator that enables the analysis of physical property changes in a model pulmonary surfactant layer at the air–liquid interface under oxidative stress condition. The chemical composition change of the phospholipid mixture under oxidative stress in the air–liquid interface was identified visually through fluorescence monitoring. Chemical compositional changes induce a model PS lipid monolayer under oxidative stress to become more elastic and increase dynamic viscosity of the surfactant layer. We observed their effects in terms of the bubble size and the oscillatory formation process. Ozone exposure is known to affect breathing and pulmonary functions, including alteration of the respiratory rate, decrease of tidal volume and airflow limitation.[31–34] The observed chemical composition changes followed by physical property alterations may play a critical role in such symptoms. Also in the PS system, regulating the surface viscosity by condensing or removing unsaturated lipids has been reported as an important role for SP-C, one of the lung surfactant specific proteins, to prevent lung dysfunction. Thus, a lack of one of the major components of the PS system, such as POPG as we studied, can be a potential source of lung damage over time.[35] Our platform was validated for its potential use in studying the physical characteristics of the interface resulting from chemical reactions at the interface. Due to the sensitive response, reproducibility for good statistics and the ease of manipulation/analysis, we believe that microbubbles in microfluidics have a potential in understanding the interfacial physics, as well as chemistry of the various surfactant systems.

Acknowledgements

This work is supported by the Basic Science Research Program (Grant No. 2010-0021508, H. I. K., P. I.) through the National Research Foundation (NRF) of Korea funded by the Ministry of Education, Science and Technology and by the National Cancer Institute Grant No. 5U54 CA119347 (J. R. H., P. I.).

References

1 A. B. Theberge, F. Courtois, Y. Schaerli, M. Fischlechner, C. Abell, F. Hollfelder and W. T. Huck, *Angew. Chem. Int. Ed.*, 2010, **49**, 5846–5868.
2 R. Tewhey, J. B. Warner, M. Nakano, B. Libby, M. Medkova, P. H. David, S. K. Kotsopoulos, M. L. Samuels, J. B. Hutchison, J. W. Larson, E. J. Topol, M. P. Weiner, O. Harismendy, J. Olson, D. R. Link and K. A. Frazer, *Nat. Biotechnol.*, 2009, **27**, 1025–1031.
3 R. R. Pompano, W. Liu, W. Du and R. F. Ismagilov, *Annu. Rev. Anal. Chem.*, 2011, **4**, 59–81.
4 T. Osaki, S. Yoshizawa, R. Kawano, H. Sasaki and S. Takeuchi, *Anal. Chem.*, 2011, **83**, 3186–3191.
5 J. E. Kreutz, L. Li, L. S. Roach, T. Hatakeyama and R. F. Ismagilov, *J. Am. Chem. Soc.*, 2009, **131**, 6042–6043.
6 A. Huebner, L. F. Olguin, D. Bratton, G. Whyte, W. T. S. Huck, A. J. de Mello, J. B. Edel, C. Abell and F. Hollfelder, *Anal. Chem.*, 2008, **80**, 3890–3896.
7 J. Q. Boedicker, M. E. Vincent and R. F. Ismagilov, *Angew. Chem., Int. Ed.*, 2009, **48**, 5908–5911.
8 J. Park, A. Kerner, M. A. Burns and X. N. Lin, *PLoS One*, 2011, **6**, e17019.

9 K. Hettiarachchi, E. Talu, M. L. Longo, P. A. Dayton and A. P. Lee, *Lab Chip*, 2007, **7**, 463–468.
10 M. Seo, I. Gorelikov, R. Williams and N. Matsuura, *Langmuir*, 2010, **26**, 13855–13860.
11 M. Hashimoto, S. S. Shevkoplyas, B. Zasonska, T. Szymborski, P. Garstecki and G. M. Whitesides, *Small*, 2008, **4**, 1795–1805.
12 P. Garstecki, M. J. Fuerstman and G. M. Whitesides, *Nat. Phys.*, 2005, **1**, 168–171.
13 P. Garstecki, M. J. Fuerstman, H. A. Stone and G. M. Whitesides, *Lab Chip*, 2006, **6**, 437–446.
14 S. L. Anna, N. Bontoux and H. A. Stone, *Appl. Phys. Lett.*, 2003, **82**, 364–366.
15 M. Jerrett, R. T. Burnett, C. A. Pope 3rd, K. Ito, G. Thurston, D. Krewski, Y. Shi, E. Calle and M. Thun, *N. Engl. J. Med.*, 2009, **360**, 1085–1095.
16 J. W. Anseth, A. J. Goffin, G. G. Fuller, A. J. Ghio, P. N. Kao and D. Upadhyay, *Am. J. Respir. Cell Mol. Biol.*, 2005, **33**, 161–168.
17 *Lung Disease Data: 2008*, American Lung Association National Headquarters, New York, 2008.
18 S. Enami, M. R. Hoffmann and A. J. Colussi, *Proc. Natl. Acad. Sci. U. S. A.*, 2008, **105**, 7365–7369.
19 S. Enami, M. R. Hoffmann and A. J. Colussi, *J. Phys. Chem. B*, 2008, **112**, 4153–4156.
20 H. I. Kim, H. Kim, Y. S. Shin, L. W. Beegle, W. A. Goddard, J. R. Heath, I. Kanik and J. L. Beauchamp, *J. Phys. Chem. B*, 2010, **114**, 9496–9503.
21 D. C. Duffy, J. C. McDonald, O. J. A. Schueller and G. M. Whitesides, *Anal. Chem.*, 1998, **70**, 4974–4984.
22 P. Garstecki, I. Gitlin, W. DiLuzio, G. M. Whitesides, E. Kumacheva and H. A. Stone, *Appl. Phys. Lett.*, 2004, **85**, 2649–2651.
23 J. A. Vickers, M. M. Caulum and C. S. Henry, *Anal. Chem.*, 2006, **78**, 7446–7452.
24 P. B. Ghosh and M. W. Whitehouse, *Biochem. J.*, 1968, **108**, 155–156.
25 T. Thorsen, R. W. Roberts, F. H. Arnold and S. R. Quake, *Phys. Rev. Lett.*, 2001, **86**, 4163–4166.
26 M. F. A. Hendrickx and C. Vinckier, *J. Phys. Chem. A*, 2003, **107**, 7574–7580.
27 Z. D. Wang, S. B. Hall and R. H. Notter, *J. Lipid. Res.*, 1995, **36**, 1283–1293.
28 M. W. Hawco, P. J. Davis and K. M. W. Keough, *J. Appl. Physiol.*, 1981, **51**, 509–515.
29 A. Gopal and K. Y. C. Lee, *J. Phys. Chem. B*, 2001, **105**, 10348–10354.
30 S. Baoukina, L. Monticelli, H. J. Risselada, S. J. Marrink and D. P. Tieleman, *Proc. Natl. Acad. Sci. U. S. A.*, 2008, **105**, 10803–10808.
31 R. B. Devlin, W. F. McDonnell, S. Becker, M. C. Madden, M. P. McGee, R. Perez, G. Hatch, D. E. House and H. S. Koren, *Toxicol. Appl. Pharmacol.*, 1996, **138**, 176–185.
32 W. D. Currie, S. van Schaik, I. Vargas and G. Enhorning, *Eur. Respir. J.*, 1998, **12**, 288–293.
33 W. D. Currie, S. M. van Schaik, I. Vargas and G. Enhorning, *Toxicology*, 1998, **125**, 21–30.
34 G. Enhorning, *Chest*, 2008, **133**, 975–980.
35 C. Alonso, A. Waring and J. A. Zasadzinski, *Biophys. J.*, 2005, **89**, 266–273.

